X-ray diffraction study of the single-crystal elastic moduli of ϵ-Fe up to 30 GPa

Sébastien Merkel,[1,2,3] Jinfu Shu,[1] Philippe Gillet,[2]
Ho-Kwang Mao,[1] and Russell J. Hemley[1]

Received 1 June 2004; revised 3 February 2005; accepted 11 February 2005; published 13 May 2005.

[1] Room temperature investigations of the single-crystal elastic moduli and anisotropy of the ϵ phase of iron are performed up to 30.3 GPa using the radial X-ray diffraction technique. The accuracy of the calculated elastic moduli has improved compared to previous measurements using similar techniques because of an increase in accuracy of the measurement, confinement of the sample to limit the effect of plasticity, and better calibration of the stress conditions. The aggregate shear modulus that we obtain is in good agreement with a variety of other experimental deductions but differs from first-principles calculations. The effects of the calibration of stress and micromechanical model on the deduction of elastic moduli and elastic anisotropy are discussed in detail. The anisotropy we obtain has the same order of magnitude as first-principles calculations but the direction is reversed, with a weaker amplitude that previous measurements.

Citation: Merkel, S., J. Shu, P. Gillet, H.-K. Mao, and R. J. Hemley (2005), X-ray diffraction study of the single-crystal elastic moduli of ϵ-Fe up to 30 GPa, *J. Geophys. Res.*, *110*, B05201, doi:10.1029/2004JB003197.

1. Introduction

[2] Understanding the effect of pressure on the propagation of elastic waves in solid materials is of fundamental interest for constraining the properties of the deep interior of the planets. To that extent, the elastic properties of iron and their pressure dependence are particularly important as it is the main constituent of the Earth inner core. Although the crystal structure of iron at these depths is still debated, it is accepted that the ϵ phase has a wide stability field and serves as a starting point for modeling the inner core [*Hemley and Mao*, 2001]. However, constraining the elastic properties of this phase remains a challenging task, both experimentally and using first-principles calculations.

[3] The compression curve of ϵ-Fe has been measured experimentally up to core pressures, using both static and dynamic methods, and is particularly well constrained [*Brown and McQueen*, 1986; *Jephcoat et al.*, 1986; *Mao et al.*, 1990; *Yoo et al.*, 1993; *Nguyen and Holmes*, 1998, 2004; *Ma et al.*, 2004]. From these data, an estimation of both the variation of density and bulk modulus with pressure can be obtained. On the other hand, first-principles calculations of the equation of state of ϵ-Fe are difficult, especially at low pressure [*Stixrude et al.*, 1994; *Steinle-Neumann et al.*, 1999]. The discrepancy between experimental data and the results from first-principles calculations is larger than what is typically obtained for other transition metals. Inclusion of magnetic effects is thought to improve the agreement with experiments but the density remains overestimated, and there are fundamental aspects of the physics of ϵ-Fe affecting first-principles calculations that are not well understood [*Jarlborg*, 2002; *Bose et al.*, 2003; *Thakor et al.*, 2003; *Gannarelli et al.*, 2003; *Steinle-Neumann et al.*, 2004].

[4] The aggregate compressional wave velocity V_P of ϵ-Fe has been obtained up to 110 GPa using inelastic X-ray scattering [*Fiquet et al.*, 2001; *Antonangeli et al.*, 2004]. This represented the first direct measurement of acoustic sound velocity up to core pressure under static conditions. Other determination of aggregate elastic moduli include measurement of the shear modulus of ϵ-Fe at 16 GPa using ultrasonic interferometry [*Mao et al.*, 1998], deduction of both the aggregate compressional and shear wave velocities using high-pressure and high-temperature X-ray diffraction and Rietveld refinement [*Dubrovinsky et al.*, 2001], as well as measurements of phonon density of states [*Lübbers et al.*, 2000; *Mao et al.*, 2001].

[5] Measurements of single-crystal elastic moduli of ϵ-Fe are scarce. Constraints on elastic moduli by inverting X-ray diffraction data on polycrystals under nonhydrostatic stress have been reported twice [*Singh et al.*, 1998b; *Mao et al.*, 1998]. However, the calibration of stresses in theses sample was problematic and the effect of lattice preferred orientation was difficult to constrain [*Matthies et al.*, 2001a]. Several sets of first-principles calculations have also been performed [*Stixrude and Cohen*, 1995; *Söderlind et al.*, 1996; *Cohen et al.*, 1997; *Steinle-Neumann et al.*, 1999; *Laio et al.*, 2000; *Vočadlo et al.*, 2003]. Finally, the C_{44} elastic modulus of ϵ-Fe and its pressure dependence were deduced from Raman measurements using a phenomeno-

[1]Geophysical Laboratory, Carnegie Institution of Washington, Washington, D. C., USA.
[2]Laboratoire des Sciences de la Terre, École Normale Supérieure de Lyon, Lyon, France.
[3]Now at Department of Earth and Planetary Science University of California, Berkeley, California, USA.

0148-0227/05/2004JB003197$09.00

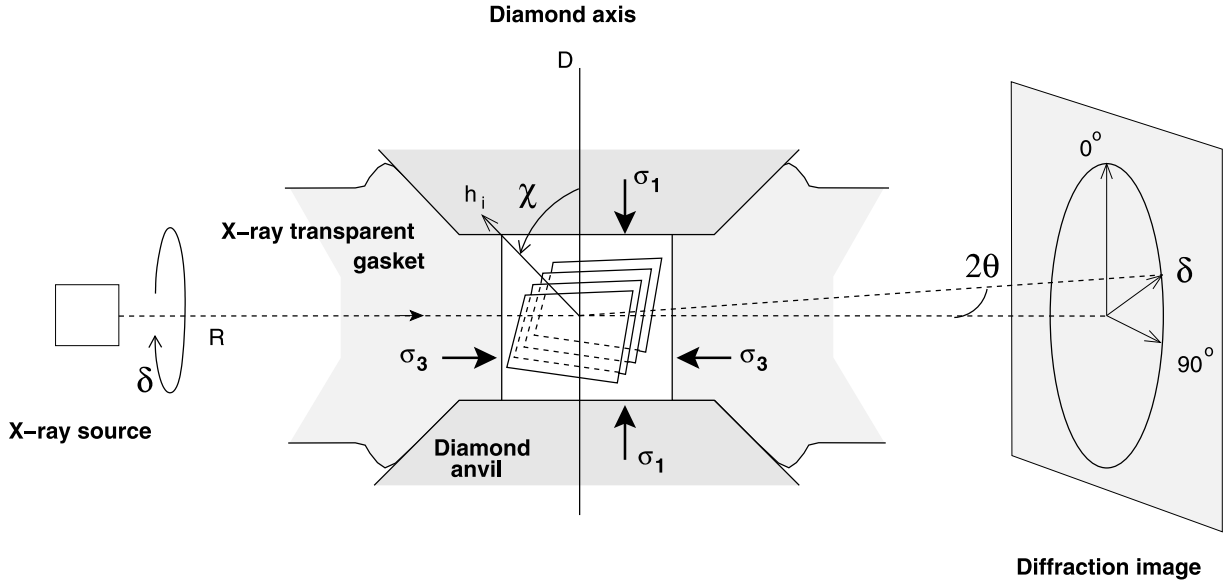

Figure 1. Schematic of the experiment. The polycrystalline sample is confined under nonhydrostatic stress conditions between the two diamond anvils. The σ_1 is the axial stress imposed by the diamonds, and σ_3 is the radial stress imposed by the gasket. A monochromatic X-ray beam is sent through the gasket with the direction of the incoming beam orthogonal to the diamond axis and the data collected on an imaging plate orthogonal to the incoming beam. The position of the diffraction lines and intensity of diffraction are analyzed as a function of the azimuthal angle δ from which we calculate the angle χ between the normal to the diffracting plane h_i and the compression direction.

logical model [*Merkel et al.*, 2000]. As shown by *Merkel et al.* [2000], there is actually no consensus on the elastic properties of iron under pressure and significant work remains to be done.

[6] In recent years, the procedure for determining the single-crystal elastic moduli from X-ray diffraction at high pressure has improved considerably. On the experimental side, the measurements can now be performed using monochromatic beams and large area detectors, allowing precise measurements of the variation of *d* spacings with orientation as well as texture analysis [*Merkel et al.*, 2002, 2003, 2004]. In addition, the theory for the inversion of elastic moduli was clarified by including effects of lattice preferred orientation in the analysis [*Matthies et al.*, 2001a, 2001b], and the C_{44} single-crystal elastic modulus of ϵ-Fe was constrained up to core pressure [*Merkel et al.*, 2000]. In this paper, we readdress the issue of the single-crystal elasticity of hcp-iron measured from X-ray diffraction using those new constrains and new experimental data.

2. Methods

2.1. Experimental Technique

[7] We perform a uniaxial deformation of a polycrystalline iron sample embedded in MgO powder with the diamond anvil cell. The stress state in the sample is analyzed using X-ray diffraction with the incident beam orthogonal to the compression axis (Figure 1). Experimental details along with the analysis of the strain state, polycrystalline texture, and deformation mechanisms of the MgO surrounding the Fe sample as well as analysis of the texture of the ϵ-Fe sample in this same experiment have been given elsewhere [*Merkel et al.*, 2002, 2004].

[8] In order to measure angle dispersive diffraction in a radial geometry, the confining gasket was made of a mixture of amorphous boron and epoxy with a ratio of 2/3 in weight. Iron samples with grain size smaller than 1 μm were used to ensure a large number of crystallites and orientations in the analysis. The samples were pressed into platelets between two large diamonds (1 mm tip diameter). A layer of MgO was deposited at the bottom of the gasket hole. A small platelet of pure polycrystalline iron was then added. Finally, another platelet of MgO was added above the Fe platelet and pressed using the diamond anvils.

[9] Diffraction experiments were conducted using angle dispersive synchrotron X-ray diffraction techniques at the ID-13 beam line of the GSECARS sector at the Advanced Photon Source. A monochromatic beam of wavelength 0.4246$\mathring{A}$ was used. Diffraction patterns were recorded with 2000×2700 pixels image plates. The raw X-ray diffraction images were corrected for nonorthogonality by comparing to a CeO_2 standard pattern taken prior to the experiment. The sample to image plate distance calibrated using the CeO_2 standard was 290.7 mm. Variations of absorption of the X-ray by the gasket as a function of the azimuthal angle were not accounted for, but they are known to be of relatively small amplitude compared to the diffraction intensities of the sample (e.g., Figure 2).

[10] In the second experiment of *Merkel et al.* [2002], MgO and Fe were compressed at 300 K up to 30.3 GPa. At this pressure we performed several laser heating cycles. During the last heating at this pressure (about 28 GPa, up to 1300 K), part of the ϵ-Fe sample converted into the γ phase (fcc). This phase is quenchable to ambient temperature and has diffraction peaks that partially overlap those of ϵ-Fe.

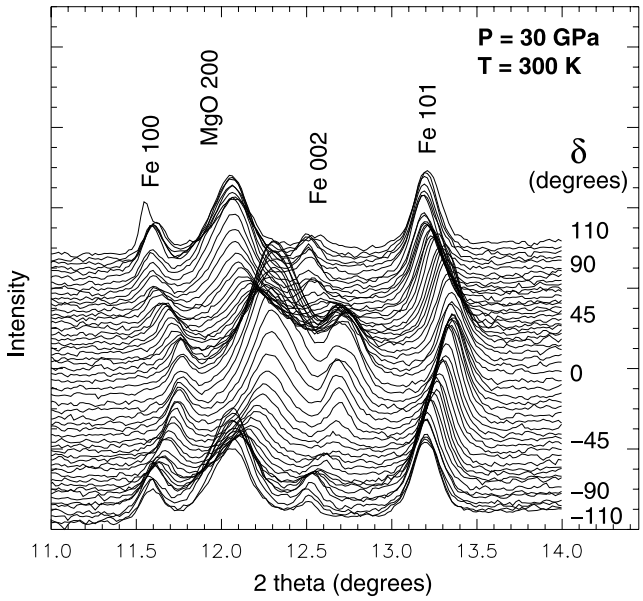

Figure 2. Patterns extracted from the diffraction image at 30.3 GPa for azimuth angles δ varying from −110° to 110°. The 2θ interval was restricted to 11–14° in order to emphasize the variations of *d* spacings and intensities of diffraction with orientation. Diffraction peaks from the pressure medium, MgO, and the iron sample are labeled.

Therefore we did not take the analysis any further and the data presented here will only extend up to 30.3 GPa and under ambient temperature. Pressures were estimated using the hydrostatic equation of state of the pressure medium, MgO [*Speziale et al.*, 2001], and iron itself [*Jephcoat et al.*, 1986], after correcting the data for the effect of nonhydrostatic stress [e.g., *Merkel et al.*, 2002]. Pressures determined from the hcp-Fe or MgO samples differed by less than 0.5 GPa for all pressures (Tables 1 and 2). Figure 2 presents examples of diffraction patterns at 30.3 GPa that were used for this analysis.

[11] As the orientation of the diamond anvil cell was not completely fixed, the origin for azimuth angles on the imaging plate was adjusted by locating the orientation at which the *d* spacings are minimum. There were slight deviations (up to a few degrees) between the minimum found for different lattice planes. However, some distortions of the same amplitude could also be observed for the calibration sample. Therefore those deviations were ignored and we chose an average value as reference for azimuth angles.

2.2. General Equations

[12] Because of the symmetry of the experiment (Figure 1), the stress conditions in the sample can be described as

$$\sigma = \begin{bmatrix} \sigma_3 & 0 & 0 \\ 0 & \sigma_3 & 0 \\ 0 & 0 & \sigma_1 \end{bmatrix} = \begin{bmatrix} P & 0 & 0 \\ 0 & P & 0 \\ 0 & 0 & P \end{bmatrix} + \begin{bmatrix} -\frac{t}{3} & 0 & 0 \\ 0 & -\frac{t}{3} & 0 \\ 0 & 0 & 2\frac{t}{3} \end{bmatrix}, \quad (1)$$

where σ_3 and σ_1 are the radial and axial stress components, respectively; P is the normal mean stress or equivalent hydrostatic pressure, and $t = (\sigma_1 - \sigma_3)$ is the maximum principal stress, which we will call the uniaxial stress throughout this paper.

[13] The *d* spacings measured by X-ray diffraction depend on the Miller indices of the lattice plane, *hkl*, the stress applied to the sample, P and t, the elastic tensor of the material under the pressure P, $[C_{ij}]$, the orientation distribution function (ODF) of the sample, f, and the direction of observation, $\mathbf{y}$,

$$\overline{d}_m = \overline{d}_m(hkl, P, t, [C_{ij}], f, \mathbf{y}), \quad (2)$$

where the overbar indicates an average over all grains contributing to the diffraction at the orientation $\mathbf{y}$. In order to analyze the effect of nonhydrostatic stress on the measured *d* spacings, it is useful to separate the contribution of the hydrostatic pressure P that does not depend on the direction of observation using

$$\overline{d}_m(hkl, P, t, [C_{ij}], f, \mathbf{y}) = d_0(hkl, P) \cdot \left[1 + \frac{\overline{d}_m(hkl, P, t, [C_{ij}], f, \mathbf{y}) - d_0(hkl, P)}{d_0(hkl, P)}\right] \quad (3)$$

$$\overline{d}_m(hkl, P, t, [C_{ij}], f, \mathbf{y}) = d_0(hkl, P)\left[1 + \overline{\epsilon}(hkl, P, t, [C_{ij}], f, \mathbf{y})\right], \quad (4)$$

where $d_0(hkl, P)$ is the *d* spacing of the plane under the equivalent hydrostatic pressure P. It can be easily related to the cell parameters a and c of the sample at pressure P.

Table 1. Elastic Moduli and Uniaxial Stress Calculated in This Study for the Reuss Bound (α = 1.0)[a]

P-MgO	P-Fe	t	C_{11}	C_{12}	C_{13}	C_{33}	C_{44}	C_{66}
17.4 ± 0.5	17.7 ± 0.5	3.03 ± 0.46	480 ± 64	85 ± 90	182 ± 35	373 ± 66	130 ± 50	197 ± 76
18.3 ± 0.5	18.5 ± 0.5	3.03 ± 0.46	419 ± 26	152 ± 19	189 ± 12	371 ± 23	131 ± 23	133 ± 22
20.2 ± 0.5	20.3 ± 0.5	3.03 ± 0.45	423 ± 24	166 ± 16	197 ± 11	381 ± 21	134 ± 22	128 ± 20
23.0 ± 0.5	22.7 ± 0.5	2.93 ± 0.42	423 ± 22	198 ± 14	192 ± 15	415 ± 28	138 ± 23	112 ± 17
23.9 ± 0.5	24.1 ± 0.5	2.91 ± 0.42	423 ± 22	211 ± 26	200 ± 27	420 ± 51	140 ± 35	106 ± 19
27.0 ± 0.5	27.2 ± 0.5	3.03 ± 0.42	444 ± 22	212 ± 12	213 ± 12	429 ± 22	145 ± 21	116 ± 16
29.8 ± 0.5	30.3 ± 0.5	3.39 ± 0.45	456 ± 21	220 ± 29	230 ± 25	432 ± 46	150 ± 40	118 ± 21
	28.8 ± 0.5	2.73 ± 0.37	441 ± 20	234 ± 24	217 ± 26	442 ± 49	148 ± 37	103 ± 17

[a]These calculations were calibrated using the compressibility measurements of *Jephcoat et al.* [1986] and C_{44} deduced from Raman spectroscopy [*Merkel et al.*, 2000]. Pressures, stresses, and elastic moduli are expressed in GPa.

Table 2. Elastic Moduli and Uniaxial Stress Calculated in this Study for the Hill Average ($\alpha = 0.5$)[a]

P-MgO	P-Fe	t	C_{11}	C_{12}	C_{13}	C_{33}	C_{44}	C_{66}
17.4 ± 0.5	17.7 ± 0.5	3.60 ± 0.55	584 ± 178	−24 ± 224	190 ± 47	351 ± 83	130 ± 90	304 ± 201
18.3 ± 0.5	18.5 ± 0.5	2.90 ± 0.44	415 ± 29	144 ± 29	203 ± 11	339 ± 20	131 ± 28	136 ± 28
20.2 ± 0.5	20.3 ± 0.5	2.82 ± 0.41	410 ± 24	165 ± 22	213 ± 10	346 ± 17	134 ± 25	122 ± 22
23.0 ± 0.5	22.7 ± 0.5	2.60 ± 0.38	397 ± 19	214 ± 19	205 ± 16	384 ± 28	138 ± 26	91 ± 17
23.9 ± 0.5	24.1 ± 0.5	2.50 ± 0.35	391 ± 18	231 ± 39	215 ± 31	385 ± 54	140 ± 44	80 ± 25
27.0 ± 0.5	27.2 ± 0.5	2.64 ± 0.36	414 ± 17	228 ± 13	230 ± 10	391 ± 18	145 ± 22	93 ± 14
29.8 ± 0.5	30.3 ± 0.5	2.88 ± 0.38	421 ± 24	238 ± 44	250 ± 24	389 ± 41	150 ± 57	91 ± 33
	28.8 ± 0.5	2.28 ± 0.31	403 ± 16	257 ± 34	234 ± 28	402 ± 49	148 ± 47	73 ± 21

[a]These calculations were calibrated using the compressibility measurements of *Jephcoat et al.* [1986] and C_{44} deduced from Raman spectroscopy [*Merkel et al.*, 2000]. Pressures, stresses, and elastic moduli are expressed in GPa.

[14] Because of the simple geometry of the experiment, the orientation dependence **y** of the measurement can be reduced to a single parameter, the angle χ between the diffracting plane normal and the load axis (Figure 1). It can be calculated from the azimuth angle on the imaging plate using the relation

$$\cos\chi = \cos\theta\cos\delta, \tag{5}$$

where θ is the diffraction angle.

[15] Several theoretical approaches have been developed in order to address the relation between those measurements and the single crystal elastic moduli of the sample and they can be divided in two categories, those which neglect the effect of lattice preferred orientation, and those which include it.

2.3. Analysis With No Effects of Preferred Orientation

[16] The resolution of the lattice strains equations for a polycrystal under uniaxial stress and no effect of texture has been developed independently by several groups [e.g., *Bollenrath et al.*, 1967; *Singh et al.*, 1998a; *Bittorf et al.*, 1998; *Gnäupel-Herold et al.*, 1998; *Howard and Kisi*, 1999, and references therein]. In this paper, we will refer to the specific application to high-pressure experiments, as described by *Singh et al.* [1998a].

[17] If we assume that the crystallites in the sample are randomly oriented, the equations of linear elasticity provide

$$\bar{\epsilon}(hkl, P, t, [C_{ij}], \chi) = (1 - 3\cos^2\chi)Q(hkl, P, t, [C_{ij}]), \tag{6}$$

where $Q(hkl, P, t, [C_{ij}])$ is given by

$$Q(hkl, P, t, [S_{ij}]) = \frac{t}{3}\left[\frac{\alpha}{2\,G_R(hkl, [S_{ij}])} + \frac{1-\alpha}{2\,G_V([S_{ij}])}\right], \tag{7}$$

where $[S_{ij}]$ is the elastic compliances tensor, and $G_R(hkl)$ and G_V are appropriate moduli of the aggregate under the Reuss (isostress) and Voigt (isostrain) approximations, respectively, and do not depend on the direction of observation. The factor α, which lies between 0 and 1, determines the relative weight of isostress (Reuss) and isostrain (Voigt) conditions. It specifies the degree of stress and strain continuity across grains in the sample.

[18] For a hexagonal crystal, we have

$$\begin{aligned}\frac{1}{G_R(hkl)} &= (2S_{11} - S_{12} - S_{13}) \\ &+ (-5S_{11} + S_{12} + 5S_{13} - S_{33} + 3S_{44})l_3^2(hkl, P) \\ &+ (3S_{11} - 6S_{13} + 3S_{33} - 3S_{44})l_3^4(hkl, P),\end{aligned} \tag{8}$$

$$\frac{1}{2G_V} = \frac{15}{C_{11} + C_{12} + 2C_{33} - 4C_{13} + 12C_{44} + 12C_{66}}, \tag{9}$$

where

$$l_3^2(hkl, P) = \frac{3a^2l^2}{4c^2(h^2 + hk + k^2) + 3a^2l^2}, \tag{10}$$

where a and c are the cell parameters at pressure P. Therefore, for the hexagonal symmetry, we expect a quadratic relation between $Q(hkl, P, t, [S_{ij}])$ and $l_3^2(hkl, P)$ that can provide three independent coefficients m_0, m_1 and m_2 function of the uniaxial stress t, the parameter α and the representative single-crystal elastic moduli $[C_{ij}]$. Two additional constrains are provided by the compressibilities in directions a and c,

$$\chi_a = \alpha(S_{11} + S_{12} + S_{13}) + (1 - \alpha)\frac{1}{3K_V} \tag{11}$$

$$\chi_c = \alpha(S_{33} + 2S_{13}) + (1 - \alpha)\frac{1}{3K_V} \tag{12}$$

that can be deduced from equation of state measurements using

$$2\chi_a + \chi_c = \frac{1}{K}, \quad \chi_a - \chi_c = \left(\frac{\partial \ln(c/a)}{\partial P}\right). \tag{13}$$

Therefore we have a system of five independent equations

$$\begin{aligned} m_0 &= \frac{\alpha t}{6}\left[(2S_{11} - S_{12} - S_{13}) + \frac{1-\alpha}{\alpha}\frac{1}{2G_V}\right], \\ m_1 &= \frac{\alpha t}{6}(-5S_{11} + S_{12} + 5S_{13} - S_{33} + 3S_{44}), \\ m_2 &= \frac{\alpha t}{6}(3S_{11} - 6S_{13} + 3S_{33} - 3S_{44}), \\ \chi_a &= \alpha(S_{11} + S_{12} + S_{13}) + (1 - \alpha)\frac{1}{3K_V}, \\ \chi_c &= \alpha(S_{33} + 2S_{13}) + (1 - \alpha)\frac{1}{3K_V} \end{aligned} \tag{14}$$

that can be used to solve the inverse problem and deduce the effective single-crystal elastic moduli of the polycrystal from the X-ray diffraction data.

2.4. Analysis With Effects of Preferred Orientation

[19] The resolution of the lattice strains equations for a polycrystal under uniaxial stress that considers the effects of texture have been described previously [*Matthies et al.*, 2001a, 2001b]. However, the complexity of this numerical approach has considerably limited its application.

[20] In order to consider the effect of lattice preferred orientation on the radial diffraction measurements, one has to introduce the ODF, $f(g)$, that describes the probability density to expect crystallites that have an orientation g within dg. The observed lattice strains can be described as

$$\bar{\epsilon}(hkl, P, t, [C_{ij}], f, \chi) = \bar{S}(hkl, P, t, [C_{ij}], f, \chi) \cdot \bar{\sigma}(hkl, P, t, [C_{ij}], f, \chi), \quad (15)$$

where $\bar{S}$ and $\bar{\sigma}$ are effective macroscopic elastic moduli and stresses. The effective macroscopic quantities $\bar{\epsilon}$, $\bar{S}$ and $\bar{\sigma}$ and their microscopic equivalent can be related by the equation

$$\bar{\epsilon} = \overline{\epsilon(g)} = \int_G \epsilon(g) f(g) \bar{d}g = \overline{S(g)\sigma(g)} = \bar{S}\bar{\sigma}. \quad (16)$$

The quantities measured experimentally are the macroscopic strain $\bar{\epsilon}$ and stress $\bar{\sigma}$. Therefore the deduction of the effective macroscopic elastic moduli $\bar{S}$ is direct. However, in this study, we are interested in deducing of the single-crystal elastic moduli of the material, that is the microscopic elastic properties S.

[21] The extraction of the single-crystal elastic moduli from equation (16) depends on the micromechanical model assumed for the grain interactions and no analytical relation is in general available. This inverse problem is nonlinear, and a theory used to perform the numerical inversions described in detail by *Matthies et al.* [2001b]. These authors demonstrated that with high-quality diffraction data, well-calibrated stress conditions, and no plastic deformation, elastic moduli with reasonable agreement with measurements from other techniques can be extracted.

3. Results

3.1. Experimental Data

[22] Figure 3 presents the variations of the d spacings measured for the (101) and (110) planes of ϵ-Fe with the angle χ for pressures between 17.7 and 30.3 GPa. The quality of the measurements has improved compared to previous work on this material [e.g., *Matthies et al.*, 2001a, Figure 3]: The number of measured orientations is far greater, and we can confirm that the d spacing vary almost linearly with $(1-3\cos^2\chi)$ for χ ranging between -110 and 110°, as predicted by the lattice strain theory without effect of preferred orientation (equation (6)). However, the oscillations between different orientations remain large, thus undermining the possibility of using the theory including effects of lattice preferred orientation.

3.2. Effect of Texture on the Deduced Elastic Moduli

[23] As described previously, the sample in this experiment did exhibit some degree of lattice preferred orientation

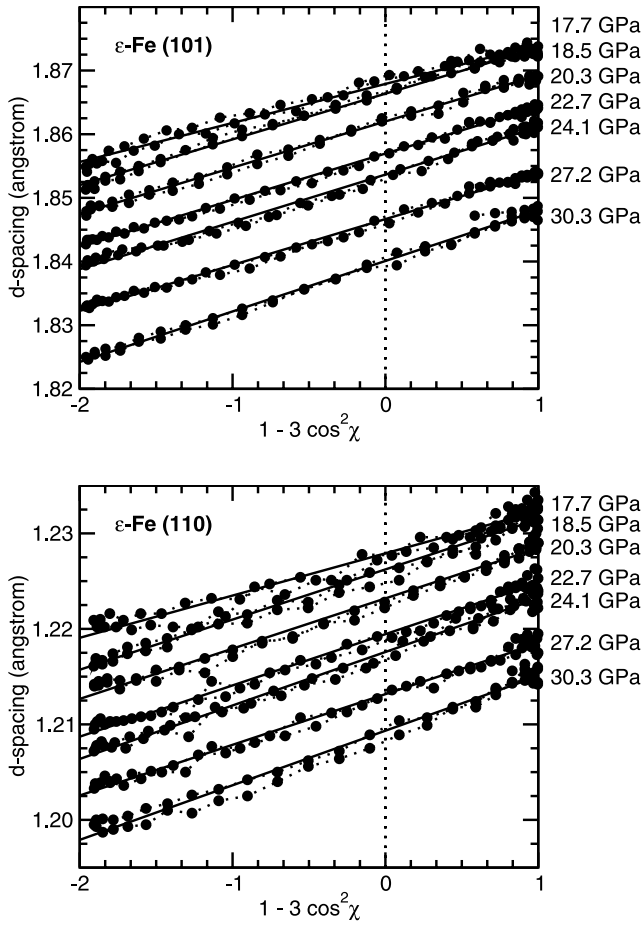

Figure 3. Dependence of the d spacings on $(1-3\cos^2\chi)$ for the (101) and (110) planes of ϵ-Fe and different pressures. Circles are experimental data and solid lines linear regressions to the data.

[*Merkel et al.*, 2004]. At this point, several factors need to be emphasized. First, the effect of lattice preferred orientation on the variation of d spacings with orientation is relatively small, on the order of 0.1%. This is actually lower than the dispersion in the experimental data presented here. Second, in the analysis of *Matthies et al.* [2001a], the model ODF that was used showed a maximum of 18.3 m.r.d. (multiples of a random distribution). The ODF fitted to the data corresponding to this sample showed a maximum of 3.51 m.r.d., so the effect of preferred orientation will be even smaller. Therefore the application of the nonlinear regressions procedures that include the effect of preferred orientation on these data is difficult. We applied these techniques but were not successful in obtaining convergence of the numerical algorithms. The influence of lattice preferred orientation on the calculated single-crystal elastic moduli is important but cannot be quantitatively assessed with the present accuracy of data acquisition. Moreover, the imaging plate system used in the measurement of these data did show some signs of distortion that does not influence results that neglect the effect of lattice preferred orientation but would certainly influence the results of the methods that do include it. Therefore all the analysis presented here will not consider the effect of lattice preferred orientation and

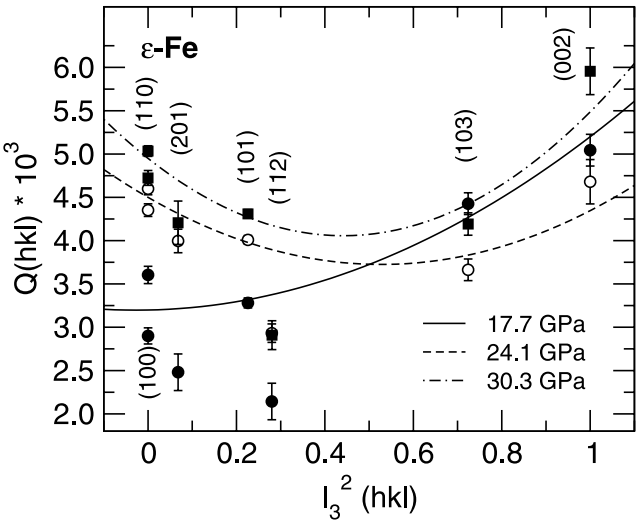

Figure 4. Amplitude of elastic strain $Q(hkl)$ versus $l_3^2(hkl)$ for ϵ-Fe at 17.7, 24.1, and 30.3 GPa. Lines are second-order polynomial fits to the data. Lattice strain theory without effects of lattice preferred orientation predicts a quadratic relation between $Q(hkl)$ and $l_3^2(hkl)$. Values of Q obtained for (201) and (112) systematically deviate from the rest of the data and are not included in the analysis (see text).

will be done using the theory described by *Singh et al.* [1998a].

3.3. Deduction of Elastic Moduli: Parametric Approach

[24] Figure 4 presents the parameters $Q(hkl)$ obtained by fitting equation (6) to the experimental data at 17.7, 24.1, and 30.3 GPa. According to the lattice strains theory of polycrystals under uniaxial stress without effect of preferred orientation, we should observe a quadratic relation between $Q(hkl)$ and l_3^2 (equations (7)–(10)). The results obtained for the (112) and (201) lattice planes showed a large systematic deviation from the rest of the data. However, those planes have a low d spacing and their diffraction lines where on the edge of the imaging plate we used. In that region, it could be seen from the calibration that there were some geometrical distortions that could not be corrected. Thus they were removed from the analysis. For the other planes the quadratic relation expected from the theory is observed to the first order. With increasing pressure, the shape of the parabola evolves considerably but it remains oriented in the same direction.

[25] In order to solve the equations from the lattice strain theory, one needs to constrain the compressibilities in direction a and c, χ_a and χ_c, respectively. We used the equation of state measured under hydrostatic conditions in our pressure range [*Jephcoat et al.*, 1986] with $K_0 = 166.6 \pm 27.9$ GPa, $K'_0 = 4.98 \pm 0.98$ and $c/a = 1.606(2) - 0.00012(3)P$. Inverting the lattice strains equations for single-crystal elastic moduli also requires the calibration of two other parameters: the uniaxial stress, $t = \sigma_1 - \sigma_3$, and the parameter α that specify the degree of stress and strain continuity within the sample.

[26] Figure 5 presents a parametric study of the elastic moduli calculated at 30.3 GPa for t between 0 and 10 GPa, $\alpha = 1.0$ (Reuss average) and $\alpha = 0.5$ (Hill average). The error bars are quite large especially for C_{12} and C_{33}. This is inherent to the technique. All elastic moduli show a linear dependence in t. However, it should be noted that the effect of t is more pronounced for the shear elastic moduli such as C_{44} and C_{66}. Therefore they would be primarily affected by an error in the calibration of t. Finally, except for C_{33}, the results for the Reuss or the Hill averages do not differ significantly.

[27] In order to provide an estimate of the effects of t and α on the elastic anisotropy deduced from the analysis,

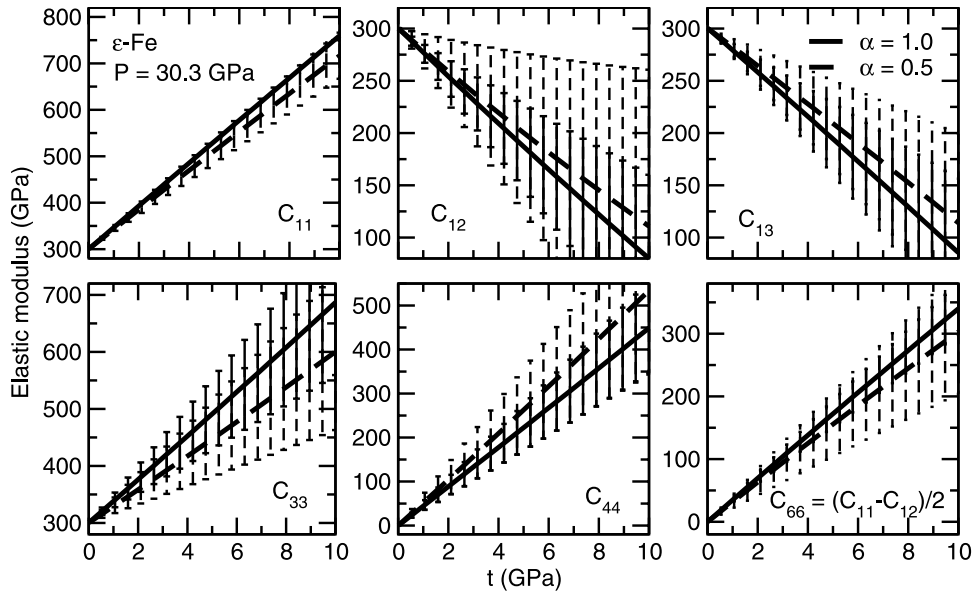

Figure 5. Parametric study on the results from the lattice strains equations for ϵ-Fe at 30.3 GPa with the uniaxial stress t varying between 0 and 10 GPa and for $\alpha = 1.0$ (Reuss bound, thick solid lines) and $\alpha = 0.5$ (Hill average, thick dashed lines). The thin solid and dashed lines are the error bars.

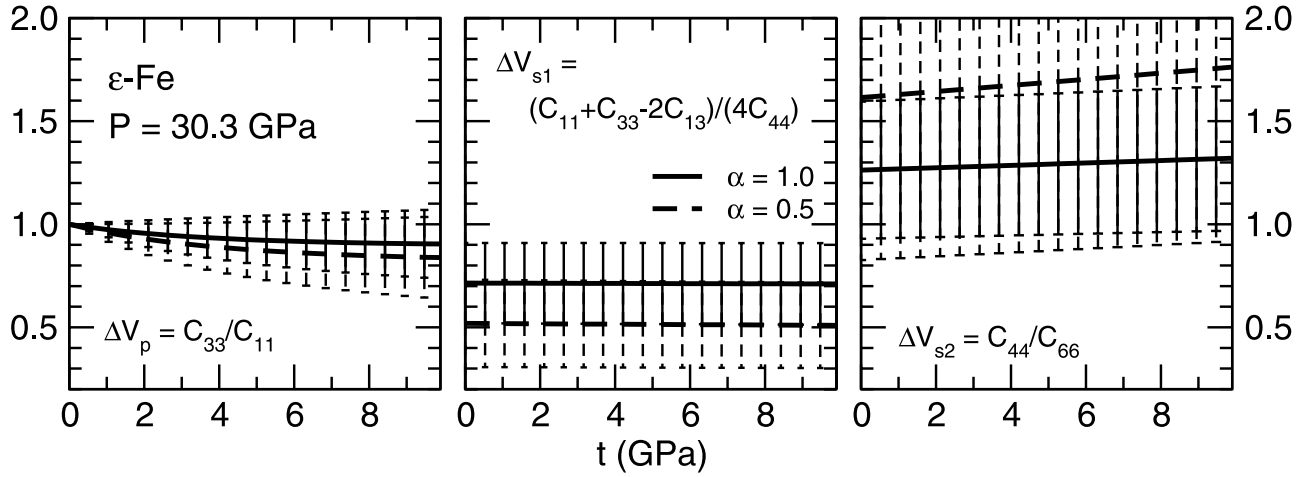

Figure 6. Parametric study of the results from the lattice strains equations for the anisotropy parameters of ϵ-Fe 30.3 GPa with the uniaxial stress t varying between 0 and 10 GPa and for $\alpha = 1.0$ (Reuss bound, thick solid lines) and $\alpha = 0.5$ (Hill average, thick dashed lines). The thin solid and dashed lines are the error bars.

Figure 6 presents the influence of t and α on the anisotropy parameters Δ_{VP}, Δ_{VS1}, and Δ_{VS2} defined as

$$\Delta_i = \frac{M_i[\mathbf{n}_x]}{M_i[100]}, \tag{17}$$

where $M = \rho V^2$ is a propagation modulus and $\mathbf{n}_x$ the extremal direction of propagation other than [100]. The index P relates to the compression wave, $S1$ to the shear wave polarized perpendicularly to the basal plane, and $S2$ to the shear wave polarized parallel to the basal plane. Δ_{VS1}, and Δ_{VS2} are good representations of the amplitude of the anisotropy for $S1$ and $S2$ waves. On the other hand, Δ_{VP} should be taken with caution as it only measures the differences between waves traveling along the a and c axis. P waves could also have extrema in an intermediary direction. We find that for our measurements, ΔV_P is almost independent of t and α. ΔV_{S1} does not depend on t and only weakly on α. ΔV_{S2} is more problematic, error bars are large and the cases with $\alpha = 1.0$ and $\alpha = 0.5$ are very different.

[28] The last step is to calibrate the value of the uniaxial stress. The use of a shear elastic modulus such as C_{44} or $C_{66} = \frac{1}{2}(C_{11} - C_{12})$ is preferable, as they vary considerably with t. In a typical nonhydrostatic diamond anvil cell experiment, errors in the calibration of stress using an external standard can be at best reduced to about 1 GPa. As shown in Figure 5, a 1 GPa error in the calibration of t will have dramatic effects on the estimation of elastic moduli, especially for low shear strength materials such as iron. This should therefore be treated with caution.

3.4. Constraints From Raman Spectroscopy

[29] Raman spectroscopy can be used to deduce one of the elastic moduli of iron, C_{44}. In a previous study, *Merkel et al.* [2000] measured the Raman spectrum of iron up to 150 GPa and used it to calculate C_{44}. A second-order linear regression on those results gives

$$C_{44} = 100.11 + 1.7198P - 0.0025104P^2, \tag{18}$$

where C_{44} and P are in GPa. The accuracy of the model depends on the assumption of a sine function for the dispersion curve of the appropriate acoustic phonon branch. It has been shown for a large number of metals for which both measurements are available that the error is on the order of ±15% [*Olijnyk et al.*, 2001]. Therefore, in the rest of this work, we will assume an error of ±20 GPa in C_{44} for the calibration of t. This error on C_{44} converts to an error of 0.3 to 0.5 GPa for t (Tables 1 and 2), and it was included in the rest of the analysis.

[30] Figure 7 shows the evolution of the uniaxial stress in ϵ-Fe with pressure deduced for $\alpha = 1.0$ and $\alpha = 0.5$. For all pressures, t remains between 2.5 and 3.5 GPa, in agreement with previous estimations [*Singh et al.*, 1998b]. Between 18 and 25 GPa, we observe a decrease of uniaxial stress, measured both in the sample and MgO, the pressure medium [*Merkel et al.*, 2002]. This is attributed to a

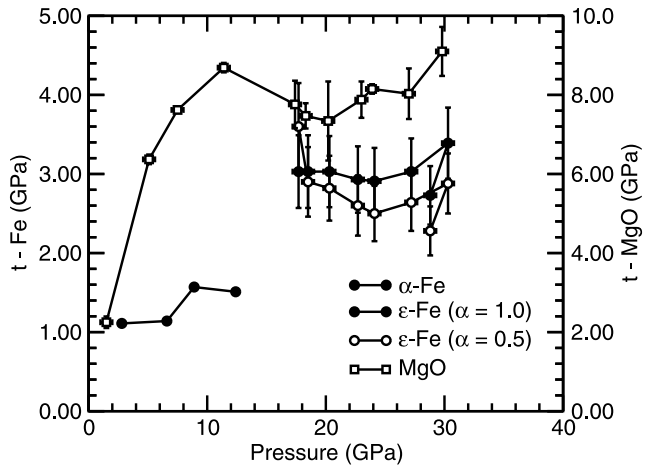

Figure 7. Uniaxial stress t in ϵ-Fe estimated using C_{44} from Raman spectroscopy for the Reuss bound ($\alpha = 1.0$) and the Hill average ($\alpha = 0.5$). For comparison, results obtained for the pressure medium, MgO, are also shown.

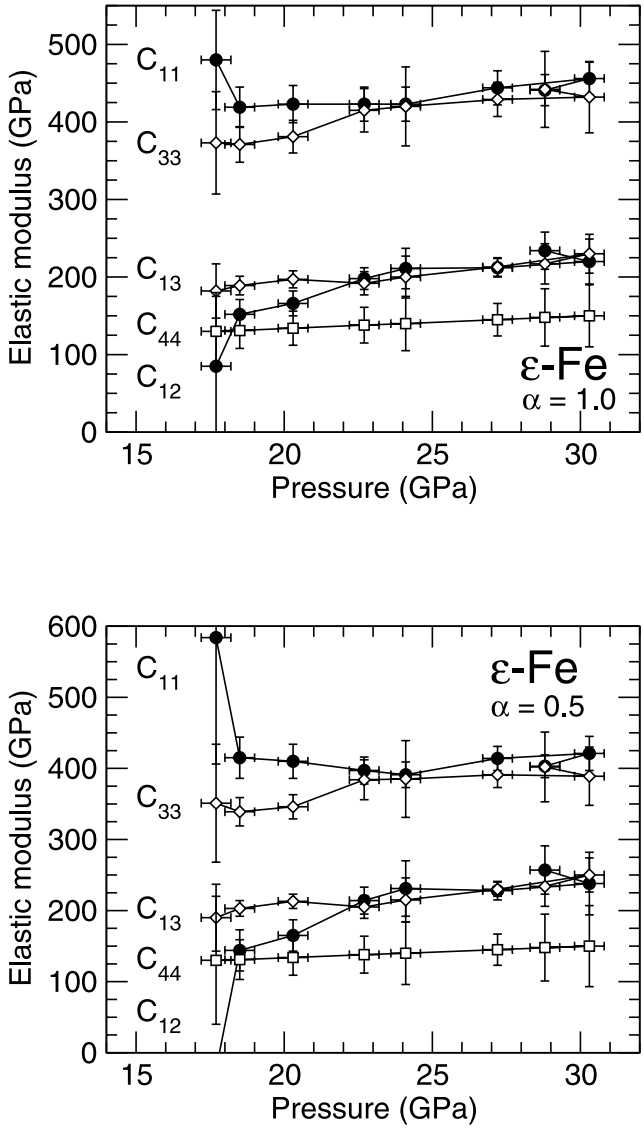

Figure 8. Elastic moduli obtained for the Reuss bound (α = 1.0) and the Hill average (α = 0.5) calibrating the uniaxial stress using C_{44} deduced from Raman spectroscopy.

rearrangement of the samples after the change of sample volume due to the transition from α- to ϵ-Fe.

[31] Figure 8 and Tables 1 and 2 present the sets of elastic moduli we obtain for α = 1.0 and α = 0.5 for all pressures in this study. At 17.7 GPa, just after the phase transition to the ϵ phase, the results show variability. This is probably related to the fact that the phase transition was not fully completed, although no evidence of α phase could be observed in the diffraction image. After the phase transition, we observe a very smooth evolution of the elastic moduli with pressure that support the self-consistency of the measurements.

4. Discussion

4.1. Elastic Moduli

[32] The reliability of the measurements of elastic moduli using radial X-ray diffraction has been subject to discussion in the literature. It has been shown in ambient pressure studies that elastic moduli obtained by X-ray diffraction for hexagonal metals can be in reasonable agreement with other techniques for polycrystals that do not suffer plastic deformation [*Matthies et al.*, 2001b]. For materials with cubic symmetry, there is also an overall good agreement between the results of X-ray diffraction and Brillouin scattering under pressure [*Merkel et al.*, 2002]. If the sample undergoes plastic deformation, new difficulties arise as microstrains induced by the deformation cannot be neglected. These result in inhomogeneities with *hkl*-dependent stress and strains that are not taken care of properly in the lattice strain analysis [*Daymond et al.*, 1999; *Weidner et al.*, 2004]. The iron samples in our experiments were confined within an MgO pressure medium. The texture measured for both samples indicate that the pressure medium MgO displayed a much higher level of lattice preferred orientation [*Merkel et al.*, 2002, 2004] and therefore absorbed a large portion of the plastic deformation. Therefore we infer that the plastic deformation applied to the iron sample was reasonably small (e.g., in comparison with previous experiments). However, we do not have any direct mean by which to investigate this hypothesis, and these approximations are likely to be the largest source of error in this analysis.

[33] A comparison with previous measurements on ϵ-Fe is not trivial. The pressures that have been studied range from 15 to 400 GPa and results can differ by a factor of two to three. Table 3 presents the elastic moduli obtained in this study, previous radial diffraction experiments [*Singh et al.*, 1998b; *Mao et al.*, 1998], as well as ab initio calculations [*Stixrude and Cohen*, 1995; *Söderlind et al.*, 1996; *Cohen et al.*, 1997; *Steinle-Neumann et al.*, 1999; *Vočadlo et al.*, 2003] in a similar pressure range. As emphasized in Table 3, the determination of the elastic moduli of iron under pressure is a delicate matter. Deviations between studies go up to 150% for C_{44}.

[34] There is a fairly good agreement on the order of magnitude of C_{12} and C_{13} for all techniques. For the C_{11} and C_{33} elastic moduli, values calculated using first-principles techniques tend to be significantly larger than those deduced from the lattice strain measurements at the same pressure. First-principles calculations are known to overestimate the incompressibility of iron for pressures below 50 GPa [*Stixrude et al.*, 1994; *Söderlind et al.*, 1996; *Steinle-Neumann et al.*, 1999]. It has been proposed that the disagreement is related to the magnetic properties of iron in the ϵ phase in the lower-pressure region of its stability field [*Steinle-Neumann et al.*, 2004]. C_{11} and C_{33} are the most relevant elastic moduli for the determination of incompressibility. Therefore the disagreement between the results from experimental studies and first-principles calculations for these elastic moduli are not surprising. First-principles calculations and the radial diffraction experiments agree on C_{12} and C_{13}, and the elastic moduli from the radial diffraction include the experimental compressibilities. Therefore we infer that the first-principles calculations overestimate C_{11} and C_{33}.

[35] The case of C_{44} remains difficult. In the previous radial diffraction studies, the uniaxial stress was calibrated using external standards or assumptions about the shear modulus of iron under pressure. As demonstrated in Figure 5, this can have dramatic effects on the estimation of C_{44}. The C_{44} deduced from Raman spectroscopy was found to be in

Table 3. Comparison Between Elastic Moduli and Seismic Wave Anisotropies Obtained in This Study for the Reuss ($\alpha = 1.0$) and Hill ($\alpha = 0.5$) Averages and Previous Experiments and Calculations in the Same Pressure Range[a]

	V	P	C_{11}	C_{12}	C_{13}	C_{33}	C_{44}	C_{66}	$\delta V_P(0°)$	$\delta V_P(45°)$	$\delta V_{S1}(45°)$	$\delta V_{S2}(0°)$
This study												
$\alpha = 1.0$	19.6	30	456(21)	220(29)	230(25)	432(46)	150(40)	118(21)	0.97(6)	1.03(5)	0.84(13)	1.13(17)
$\alpha = 0.5$	19.6	30	421(24)	238(44)	250(24)	389(41)	150(57)	91(33)	0.96(6)	1.06(7)	0.72(16)	1.28(30)
Singh et al. [1998b]												
$\alpha = 1.0$	18.4	52	639(55)	300(55)	254(41)	648(83)	422(23)	169	1.01(8)	1.17(6)	0.68(6)	1.58(19)
$\alpha = 0.5$	18.4	52	552(65)	335(60)	301(45)	562(80)	395(30)	108	1.01(9)	1.22(8)	0.57(8)	1.91(40)
Mao et al. [1998]	19.0	39	500	275	284	491	235	212	0.99	1.12	0.67	1.44
Stixrude and Cohen [1995]	18.38	39	747	301	297	802	215	223	1.04	1.00	1.05	0.98
Söderlind et al. [1996]	17.22	40	908	272	353	862	250	318	0.97	0.98	1.03	0.89
Cohen et al. [1997]		50	800	320	320	845	220	240	1.03	0.99	1.07	0.96
Steinle-Neumann et al. [1999]												
LDA	17.76	50	860	280	260	950	235	290	1.05	0.99	1.17	0.90
GGA	17.76	50	930	320	295	1010	260	305	1.04	0.98	1.14	0.92
Vočadlo et al. [2003]	18.34		672	189	264	796	210	242	1.09	1.03	1.05	0.93
Vočadlo et al. [2003]	17.34		815	252	341	926	247	282	1.07	1.02	1.03	0.94

[a]Radial diffraction measurements [*Singh et al.*, 1998b; *Mao et al.*, 1998] and first-principle [*Stixrude and Cohen*, 1995; *Söderlind et al.*, 1996; *Cohen et al.*, 1997; *Steinle-Neumann et al.*, 1999; *Vočadlo et al.*, 2003] were used. Elastic moduli and pressures are expressed in GPa, unit cell volumes are expressed in $Å^3$; numbers in parentheses indicate uncertainties on the last digit.

relatively good agreement with ultrasonic measurements for a series of other hcp metals [*Olijnyk et al.*, 2001]; therefore we are quite confident in the quality of our results.

4.2. Aggregate Properties

[36] Figure 9 presents the average shear modulus obtained from the present study as well as results of ultrasonic and previous radial diffraction measurements [*Mao et al.*, 1998], results of sound wave velocities deduced from X-ray inelastic scattering [*Fiquet et al.*, 2001] combined with the hydrostatic equation of state of iron [*Jephcoat et al.*, 1986], X-ray inelastic scattering measurements of the phonon densities of state [*Mao et al.*, 2001], results of Rietveld refinements based on high P-T X-ray diffraction measurements [*Dubrovinsky et al.*, 2001], and first-principles calculations [*Söderlind et al.*, 1996; *Cohen et al.*, 1997; *Steinle-Neumann et al.*, 1999].

[37] Above 18 GPa and for the Reuss approximation ($\alpha = 1.0$), the results from this study agree with the estimations from *Mao et al.* [1998, 2001] and *Dubrovinsky et al.* [2001]. They also follow the trend defined by the ultrasonic measurement at 16 GPa [*Mao et al.*, 1998]. Determinations based on sound wave velocities deduced from X-ray inelastic scattering [*Fiquet et al.*, 2001] and the hydrostatic equation of state of iron [*Jephcoat et al.*, 1986] fall slightly above the rest of the experimental data. This disagreement may originate from an incompatibility of the equation of state and velocities deduced from inelastic X-ray scattering (i.e., nonhydrostatic conditions of the later study). It could also arise from texturing effects in sample used in the inelastic X-ray scattering experiments that were not considered. All experimental results provide a much lower value of the shear modulus than first-principles calculations [*Söderlind et al.*, 1996; *Cohen et al.*, 1997; *Steinle-Neumann et al.*, 1999]. This can be related to the overestimation of the C_{11} and C_{33} elastic moduli discussed above.

4.3. Anisotropy

[38] Figure 10 presents the acoustic velocities of the compression wave (V_P), the shear wave polarized perpendicular to the basal plane (V_{S1}) and shear wave polarized in the basal plane (V_{S2}) as a function of the angle of the propagation direction with respect to the c axis, θ, deduced from these measurements at 30.3 GPa using the Reuss and Hill averages, as well as previous measurements using lattice strains techniques [*Singh et al.*, 1998b; *Mao et al.*, 1998] and first-principles calculations [*Stixrude and Cohen*, 1995; *Söderlind et al.*, 1996; *Cohen et al.*, 1997; *Steinle-Neumann et al.*, 1999; *Vočadlo et al.*, 2003]. In order to provide numerical comparisons, one has to consider the

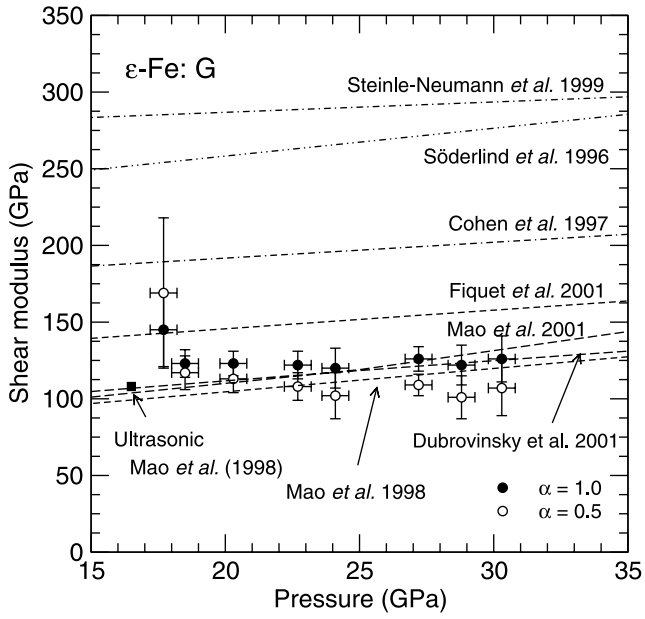

Figure 9. Aggregate shear modulus of ϵ-Fe versus P: results from this study, previous radial diffraction experiments [*Mao et al.*, 1998], ultrasonic measurement [*Mao et al.*, 1998], deduced from density of state measurements [*Mao et al.*, 2001], deduced from inelastic X-ray scattering [*Fiquet et al.*, 2001], high-pressure/high-temperature Rietveld refinement [*Dubrovinsky et al.*, 2001], and calculated by first-principles techniques [*Söderlind et al.*, 1996; *Cohen et al.*, 1997; *Steinle-Neumann et al.*, 1999].

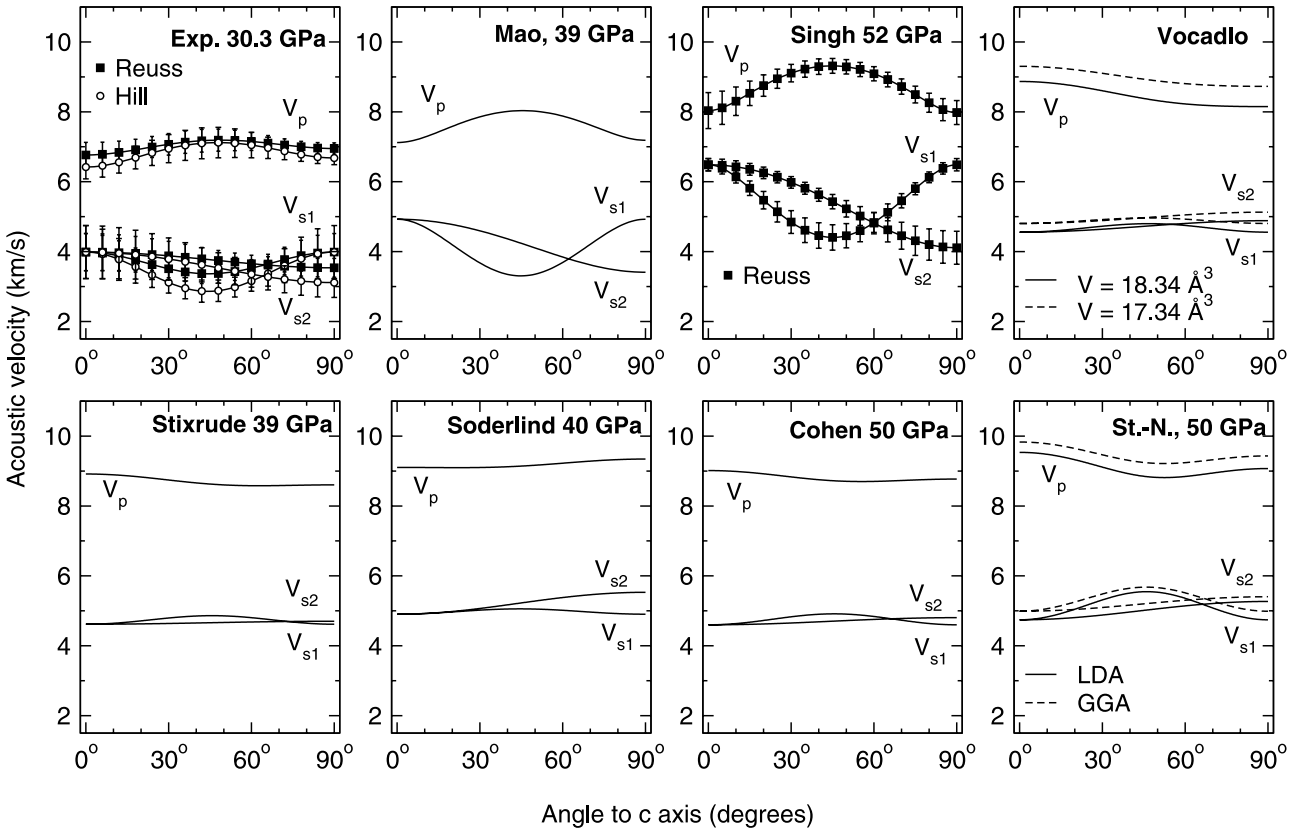

Figure 10. Seismic velocities of ϵ-Fe determined in this study at 30.3 GPa under the Reuss and Hill averages, other radial diffraction experiments [*Singh et al.*, 1998b; *Mao et al.*, 1998] and calculated using first-principles techniques [*Stixrude and Cohen*, 1995; *Söderlind et al.*, 1996; *Cohen et al.*, 1997; *Steinle-Neumann et al.*, 1999; *Vočadlo et al.*, 2003]. The *P* and *S* waves velocities are shown as a function of the angle of the direction of propagation with respect to the *c* axis. Errors are indicated, when available.

dispersion of V_P, V_{S1} and V_{S2} with θ. We introduce the parameter

$$\delta V_i(\theta) = \frac{V_i(\theta)}{V_i(90^\circ)}. \quad (19)$$

The parameter $\delta V_{S1}(45^\circ)$ is a good representation of the amplitude of the anisotropy of the *S*1 wave. Similarly, $\delta V_{S2}(0^\circ)$ can be used to discuss anisotropy of *S*2 waves. For the *P* waves however, the situation is more complex as extrema may occur for intermediate directions of propagation. According to the special dispersion of *P* waves velocities in Figure 10, we decided to represent the *P* wave anisotropy with the two parameters $\delta V_P(0^\circ)$ and $\delta V_P(45^\circ)$. Numerical results are provided in Table 3 for this experiment at 30.3 GPa, together with previous radial diffraction experiments [*Singh et al.*, 1998b; *Mao et al.*, 1998], and first-principles calculations [*Stixrude and Cohen*, 1995; *Söderlind et al.*, 1996; *Cohen et al.*, 1997; *Steinle-Neumann et al.*, 1999; *Vočadlo et al.*, 2003].

[39] The amplitude of the anisotropy obtained in this study under the Reuss bound is of the same order of magnitude than that of recent first-principles calculations [*Steinle-Neumann et al.*, 1999], e.g., 3–5% for $\delta V_P(0^\circ)$, 1–3% for $\delta V_P(45^\circ)$, 15% for $\delta V_{S1}(45^\circ)$ and 8–15% for $\delta V_{S2}(0^\circ)$. However, our uncertainties remain large and the results for the Reuss bound and Hill average differ significantly for $\delta V_{S1}(45^\circ)$ and $\delta V_{S2}(0^\circ)$.

[40] It should be noticed that all but one first-principles calculations predict $\delta V_P(45^\circ) < 1$, while all radial diffraction experiments indicate $\delta V_P(45^\circ) > 1$. Similarly, all first principles show $\delta V_{S1}(45^\circ) > 1$, while experimental results favor $\delta V_{S1}(45^\circ) < 1$. Again, $\delta V_{S2}(0^\circ) < 1$ from first-principles calculations, while $\delta V_{S2}(0^\circ) > 1$ in the experimental results. Appart from $\delta V_P(0^\circ)$, for which both experimental and theoretical calculations results vary, results from first-principles calculations and lattice strain experiments systematically provide opposite signs of anisotropy. For instance, radial diffraction experiments indicate a direction of fast polarization at $\theta = 0^\circ$ for V_{S2}, while first-principles calculations predict it at $\theta = 90^\circ$. For V_P, our results indicate that the fastest direction of propagation is located at $\theta \approx 48^\circ$ and we find $\delta V_P(48^\circ) = 1.03(5)$ for the Reuss bound and $\delta V_P(48^\circ) = 1.07(5)$ for the Hill average (an anisotropy of 3 to 7%). This is in complete agreement with recent results from inelastic X-ray scattering of textured samples that indicate that *P* waves in ϵ-Fe propagate faster by 4 to 5% at about 50° from the c axis than at 90° [*Antonangeli et al.*, 2004].

4.4. Implications for the Inner Core

[41] In considering the implications of these measurements for understanding the anisotropy of the inner core, we must emphasize that the range of pressures and temperatures

assessed in these experiments are far from those of the center of the Earth. However, we note that experimental results do differ from first-principles calculations: indeed, a fundamental understanding of iron under pressure may not yet be in hand and recent extensions of the theory need to be tested [*Steinle-Neumann et al.*, 2004]. Therefore the earlier results on elasticity and elastic anisotropy of iron under high pressure and high temperature should be treated with caution. In particular, a reversal of the anisotropy in compressed iron as a function of temperature is predicted [*Steinle-Neumann et al.*, 2001]. However, the calculated temperature dependence of the c/a ratio associated with this reversal is much larger that observed experimentally [*Ma et al.*, 2004] or predicted in other calculations [*Gannarelli et al.*, 2003].

[42] Our results indicate that the anisotropy of ϵ-Fe is lower than measured in previous radial diffraction experiments [*Singh et al.*, 1998b; *Mao et al.*, 1998]. Compared with first-principles calculations[*Stixrude and Cohen*, 1995; *Söderlind et al.*, 1996; *Cohen et al.*, 1997; *Steinle-Neumann et al.*, 1999; *Vočadlo et al.*, 2003], the locations of the directions of fast and slow polarization are systematically reversed. On the other hand, we find a good agreement with results from inelastic X-ray scattering of textured samples [*Antonangeli et al.*, 2004] with an anisotropy of 3 to 7% for P waves. This result is important for our understanding of the properties of the inner core as this measured anisotropy is comparable to that observed in the Earth (3–4%) [*Woodhouse et al.*, 1986; *Tromp*, 1993; *Song*, 1997].

5. Conclusions

[43] The elastic moduli of ϵ-Fe were determined up to 30.3 GPa using new angle dispersive radial X-ray diffraction measurements, as well as a calibration based on measurements of the hydrostatic equation of state and input from Raman spectroscopy. The resolution of the data was not sufficient to allow the inclusion of the effects of lattice preferred orientation. This approximation, as well as the neglect of the effects of plastic deformation on the stress and strain applied to each lattice planes are likely to introduce some errors in the inversion of elastic moduli. However, in the absence of additional measurements and theory, they cannot be evaluated. However, the iron sample in this experiment was confined in a pressure medium in order to limit plastic deformation and the level of texture was small. We obtain consistent values of elastic moduli up to 30.3 GPa. The average shear modulus G computed from this data is in very good agreement with a multitude of other experimental estimations. On the other hand, first-principles calculations are shown to overestimate by 100 to 200% the incompressibilities and shear modulus of iron over the same pressure range. This may arise from the neglect of the magnetic structure of iron under these conditions. The velocity anisotropy we obtain has the same order of magnitude than first principles calculations but the direction of fast and slow polarization are systematically reversed. The influence of assumptions used in the deduction of the C_{ij}, such as the micromechanical model, needs to be assessed in future works. Our results indicate that a proper calibration of the shear modulus of ϵ-Fe and its pressure dependence is now attained in the 15–50 GPa pressure range. The anisotropy parameters we calculate for P waves are in agreement with recent results from inelastic X-ray scattering of textured samples and are comparable to the anisotropy observed in the Earth. Further experiments are needed to investigate conditions closer to those of the center of the planet.

[44] **Acknowledgments.** The authors wish to thank E. Soignard and G. Shen for assistance with the experiment, S. Matthies for his input on the calculation of lattice preferred orientation effects, and S. Speziale for comments on the manuscript. Reviews by A. Kavner and an anonymous reviewer have significantly improved the manuscript. GeoSoilEnviroCARS is supported by the National Science Foundation Earth Sciences (EAR-0217473), Department of Energy Geosciences (DE-FG02-94ER14466) and the State of Illinois. Use of the APS was supported by the U.S. Department of Energy, Basic Energy Sciences, Office of Energy Research, under contract W-31-109-Eng-38. This work was also supported by the NSF (EAR-0409321 and EAR-0126009) and DOE/NNSA though the Carnegie/DOE Alliance Center (CDAC); grant DE-FC03-03NA00144.

References

Antonangeli, D., F. Occelli, H. Requardt, J. Badro, G. Fiquet, and M. Krisch (2004), Elastic anisotropy in textured hcp-iron to 112 GPa from sound wave propagation measurements, *Earth Planet. Sci. Lett.*, *225*, 243–251.

Bittorf, C., S. Matthies, H. G. Priesmeyer, and R. Wagner (1998), Diffractive determination of the thermo-elastic single crystal constants, *Intermetallics*, *7*, 1–8.

Bollenrath, F., V. Hauk, and E. H. Müller (1967), Zur berechnung der vielkristallinen elastizitätskonstanten aus den werten der einkristalle, *Z. Metall.*, *58*, 76–82.

Bose, S. K., O. V. Dolgov, J. Kortus, O. Jepsen, and O. K. Andersen (2003), Pressure dependence of electron-phonon coupling and superconductivity in hcp Fe: A linear response study, *Phys. Rev. B*, *67*, 214518.

Brown, J. M., and R. G. McQueen (1986), Phase transition, Grüneisen parameter, and elasticity for shocked iron between 77 GPa and 400 GPa, *J. Geophys. Res.*, *91*, 7485–7494.

Cohen, R. E., L. Stixrude, and E. Wasserman (1997), Tight-binding computations of elastic anisotropy of Fe, Xe, and Si under compression, *Phys. Rev. B*, *56*(14), 8575–8589.

Daymond, M., M. Bourke, and R. Von Dreele (1999), Use of Rietvelt refinement to fit hexagonal crystal structure in the presence of elastic and plastic anisotropy, *J. Appl. Phys.*, *85*, 739–747.

Dubrovinsky, L. S., N. A. Dubrovinskaia, and T. Le Bihan (2001), Aggregate sound velocities and acoustic Grüneisen parameter of iron up to 300 GPa and 1200 K, *Proc. Natl. Acad. Sci. U.S.A.*, *98*, 9484–9489.

Fiquet, G., J. Badro, F. Guyot, H. Requardt, and M. Krisch (2001), Sound velocities in iron to 100 gigapascals, *Science*, *291*, 468–471.

Gannarelli, C., D. Alfè, and M. Gillan (2003), The particle-in-cell model for ab initio thermodynamics: implications for the elastic anisotropy of the Earth's inner core, *Phys. Earth Panet. Inter.*, *139*, 243–253.

Gnäupel-Herold, T., P. C. Brand, and H. J. Prask (1998), The calculation of single crystal elastic constants for cubic crystal symmetry from powder diffraction data, *J. Appl. Crystallogr.*, *31*, 929–935.

Hemley, R. J., and H. K. Mao (2001), In situ studies of iron under pressure: New windows on the Earth's core, *Int. Geol. Rev.*, *43*, 1–30.

Howard, C. J., and E. H. Kisi (1999), Measurement of single-crystal elastic constants by neutron diffraction from polycrystals, *J. Appl. Crystallogr.*, *32*, 624–633.

Jarlborg, J. (2002), Ferromagnetic and antiferromagnetic spin fluctuations and superconductivity in the hcp-phase of Fe, *Phys. Lett. A*, *300*, 518–523.

Jephcoat, A. P., H. K. Mao, and P. M. Bell (1986), Static compression of iron to 78 GPa with rare gas solids as pressure-transmitting media, *J. Geophys. Res.*, *91*, 4677–4684.

Laio, A., S. Bernard, G. L. Chirotti, S. Scandolo, and E. Tosatti (2000), Physics of iron at Earth's core conditions, *Science*, *287*, 1027–1030.

Lübbers, R., H. F. Grünsteudel, A. I. Chumakov, and G. Wortmann (2000), Density of phonon states in iron at high pressure, *Science*, *287*, 1250–1253.

Ma, Y., M. Somayazulu, G. Shen, H. Mao, J. Shu, and R. Hemley (2004), In situ X-ray diffraction studies of iron to Earth-core conditions, *Phys. Earth Planet. Inter.*, *143–144*, 455–467.

Mao, H. K., Y. Wu, L. C. Chen, J. F. Shu, and A. P. Jephcoat (1990), Static compression of iron to 300 GPa and $Fe_{0.8}Ni_{0.2}$ alloy to 260 GPa: Implications for composition of the core, *J. Geophys. Res.*, *95*, 21,737–21,742.

Mao, H. K., J. Shu, G. Shen, R. J. Hemley, B. Li, and A. K. Singh (1998), Elasticity and rheology of iron above 220 GPa and the nature of the

Earth's inner core, *Nature*, *396*, 741–743. (Correction, Nature 399, 280, 1999.)
Mao, H. K., et al. (2001), Phonon density of state of iron up to 153 GPa, *Science*, *292*, 914–916.
Matthies, S., S. Merkel, H. R. Wenk, R. J. Hemley, and H. K. Mao (2001a), Effects of texture on the high pressure elasticity of iron from X-ray diffraction, *Earth Planet. Sci. Lett.*, *194*, 201–212.
Matthies, S., H. G. Priesmeyer, and M. R. Daymond (2001b), On the diffractive determination of single-crystal elastic constants using polycrystalline samples, *J. Appl. Crystallogr.*, *34*, 585–601.
Merkel, S., A. F. Goncharov, H. K. Mao, P. Gillet, and R. J. Hemley (2000), Raman spectroscopy of iron to 152 gigapascals: Implications for earth's inner core, *Science*, *288*, 1626–1629.
Merkel, S., H. R. Wenk, J. Shu, G. Shen, P. Gillet, H. Mao, and R. J. Hemley (2002), Deformation of polycrystalline MgO at pressures of the lower mantle, *J. Geophys. Res.*, *107*(B11), 2271, doi:10.1029/2001JB000920.
Merkel, S., H. R. Wenk, J. Badro, G. Montagnac, P. Gillet, H. K. Mao, and R. J. Hemley (2003), Deformation of (Mg,Fe)SiO_3 perovskite aggregates up to 32 GPa, *Earth Planet. Sci. Lett.*, *209*, 351–360.
Merkel, S., H. R. Wenk, P. Gillet, H. K. Mao, and R. J. Hemley (2004), Deformation of polycrystalline iron up to 30 GPa and 1000 K, *Phys. Earth Panet. Inter.*, *145*, 239–251.
Nguyen, J., and N. C. Holmes (1998), Iron sound velocities in shock waves experiments up to 400 GPa, *Eos Trans. AGU*, *79*(45), Fall Meet. Suppl., F846.
Nguyen, J., and N. Holmes (2004), Melting of iron at the physical conditions of the Earth's core, *Nature*, *427*, 339–342.
Olijnyk, H., A. P. Jephcoat, and K. Refson (2001), On optical phonons and elasticity in the hcp transition metals Fe, Ru and Re at high pressure, *Europhys. Lett.*, *53*, 504–510.
Singh, A. K., C. Balasingh, H. K. Mao, R. J. Hemley, and J. Shu (1998a), Analysis of lattice strains measured under non-hydrostatic pressure, *J. Appl. Phys.*, *83*, 7567–7575.
Singh, A. K., H. K. Mao, J. Shu, and R. J. Hemley (1998b), Estimation of single crystal elastic moduli from polycrystalline X-ray diffraction at high pressure: Applications to FeO and iron, *Phys. Rev. Lett.*, *80*, 2157–2160.
Söderlind, P., J. A. Moriarty, and J. M. Wills (1996), First-principles theory of iron to earth-core pressures: structural, vibrational and elastic properties, *Phys. Rev. B*, *53*, 14,063–14,072.
Song, X. (1997), Anisotropy of the Earth's inner core, *Rev. Geophys.*, *35*, 297–313.
Speziale, S., C. S. Zha, T. S. Duffy, R. J. Hemley, and H. K. Mao (2001), Quasi-hydrostatic compression of magnesium oxyde to 52 GPa: Implications for the pressure-volume-temperature equation of state, *J. Geophys. Res.*, *106*, 515–528.
Steinle-Neumann, G., L. Stixrude, and R. E. Cohen (1999), First-principles elastic constants for the hcp transition metals Fe, Co, and Re at high pressure, *Phys. Rev. B*, *60*(2), 791–799.
Steinle-Neumann, G., L. Stixrude, R. Cohen, and O. Gülseren (2001), Elasticity of iron at the temperature of the Earth's inner core, *Nature*, *413*, 57–60.
Steinle-Neumann, G., L. Stixrude, and R. Cohen (2004), Magnetism in dense hexagonal iron, *Proc. Natl. Acad. Sci. U.S.A.*, *101*, 33–36.
Stixrude, L., and R. E. Cohen (1995), High-pressure elasticity of iron and anisotropy of Earth's inner core, *Science*, *267*, 1972–1975.
Stixrude, L., R. E. Cohen, and D. J. Singh (1994), Iron at high pressure: Linearized-augmented-plane-wave computations in the generalized-gradient approximation, *Phys. Rev. B*, *50*, 6442–6445.
Thakor, V., J. Staunton, J. Poulter, S. Ostanin, B. Gintempo, and E. Bruno (2003), Ab initio calculations of incommensurate antiferromagnetic spin fluctuations in hcp iron under pressure, *Phys. Rev. B*, *67*(18), doi:10.1103/PhysRevB.67.180405.
Tromp, J. (1993), Support for anisotropy of the Earth's inner core from free oscillations, *Nature*, *366*, 678–681.
Vočadlo, L., D. Alfè, M. Gillan, and G. Price (2003), The properties of iron under core conditions from first principles calculations, *Phys. Earth Panet. Inter.*, *140*, 101–125.
Weidner, D., L. Li, M. Davis, and J. Chen (2004), Effect of plasticity on elastic modulus measurements, *Geophys. Res. Lett.*, *31*, L06621, doi:10.1029/2003GL019090.
Woodhouse, J. H., D. Giardini, and X. D. Li (1986), Evidence for inner core anisotropy from free oscillations, *Geophys. Res. Lett.*, *13*, 1549–1552.
Yoo, C. S., N. C. Holmes, M. Ross, D. J. Webb, and C. Pike (1993), Shock temperature, melting and phase diagram of iron at Earth core conditions, *Phys. Rev. Lett.*, *70*, 3931–3934.

P. Gillet, Laboratoire des sciences de la Terre, École normale supérieure de Lyon, 46 allée d'Italie, F-69364 Lyon Cedex 07, France.
R. J. Hemley, H.-K. Mao, and J. Shu, Geophysical Laboratory, Carnegie Institution of Washington, 5251 Broad Branch Rd., NW, Washington, DC 20015, USA.
S. Merkel, Department of Earth and Planetary Science, University of California, 307 McCone Hall, Berkeley, CA 94720-4767, USA. (smerkel@berkeley.edu)